Letter | Editors' Suggestion

Surface Luttinger arcs in Weyl semimetals

Osakpolor Eki Obakpolor and Pavan Hosur
University of Houston, Houston, Texas 77204, USA

(Received 27 August 2021; revised 12 May 2022; accepted 29 July 2022; published 15 August 2022)

The surface of a Weyl semimetal famously hosts an exotic topological metal that contains open Fermi arcs rather than closed Fermi surfaces. In this work, we show that the surface is also endowed with a feature normally associated with strongly interacting systems, namely, Luttinger arcs, defined as zeros of the electron Green's function. The Luttinger arcs connect surface projections of Weyl nodes of opposite chirality and form closed loops with the Fermi arcs when the Weyl nodes are undoped. Upon doping, the ends of the Fermi and Luttinger arcs separate and the intervening regions get filled by surface projections of bulk Fermi surfaces. Remarkably, unlike Luttinger contours in strongly interacting systems, the precise shape of the Luttinger arcs can be determined experimentally by removing a surface layer. We use this principle to sketch the Luttinger arcs for Co and Sn terminations in $Co_3Sn_2S_2$. The area enclosed by the Fermi and Luttinger arcs approximately equals the surface particle density in weakly coupled systems while the correction is governed by the interlayer couplings and the perimeter of the Fermi-Luttinger loop.

DOI: 10.1103/PhysRevB.106.L081112

Introduction. The past decade has seen tremendous advancements in the field of Weyl semimetals (WSMs)—three-dimensional (3D) materials defined by the presence of nondegenerate Bloch electron bands that intersect at arbitrary points in the Brillouin zone [1–18]. Near the intersection points, or Weyl nodes, the Bloch dispersion resembles the Weyl dispersion that is well known in high-energy physics; hence, the name WSM. The Weyl nodes carry a chirality or handedness of ± 1, emit or absorb unit Berry flux depending on their chirality, and are even in number such that the total chirality vanishes. Moreover, the nodes are topological, in the sense that they exhibit profound topological quantum anomalies, can only be destroyed by annihilating in pairs of opposite chirality, and spawn a myriad of topological transport phenomena [19–37].

WSMs famously host metallic surface states known as Fermi arcs (FAs) that connect projections of Weyl nodes of opposite chirality onto the surface Brillouin zone [8–16,38–56]. They are mandated by the bulk-boundary correspondence in topological matter analogous to the Dirac cone surface states in topological insulators [57–59]. However, the latter are exponentially localized near the surface, whereas the bulk penetration depth of the FA wave function depends strongly on its surface momentum $\boldsymbol{k}$ and diverges at its end points. The metallic nature of FAs can manifest in several ways such as quantum oscillations due to peculiar cyclotron orbits in mixed real and momentum space [52,54–56,60–63], unusual collective modes due to mixing between FAs and bulk states [64–72], and susceptibility of the surface to proximity-induced superconductivity [73–75]. However, the absence of a closed Fermi surface in the FA metal renders the Luttinger's theorem—a fundamental equality between the particle density and the volume within the Fermi surface in Fermi liquids [76–82]—inapplicable.

In this work, we show that the surface of a WSM also hosts Luttinger arcs (LAs), defined as momentum space regions where the electron Green's function vanishes. LAs and Luttinger surfaces are known to occur in strongly interacting systems due to vanishing quasiparticle weight or diverging self-energy [79,81–84]. Heuristically, LAs in WSMs can be viewed as a manifestation of strong self-interactions among surface electrons mediated by bulk states. We emphasize, however, that the system is strictly noninteracting. Interestingly, when all the Weyl nodes are undoped, the FAs and LAs form closed loops. Moreover, LAs transform into FAs when a surface layer is removed, which enables their detection. Using this idea, we determine the LAs on the (001) surface of the ferromagnetic WSM $Co_3Sn_2S_2$ [50,85–88] based on recent scanning tunneling data [87].

Surface Green's function. Let $\tilde{H}_{\boldsymbol{k}}$ denote the Bloch Hamiltonian of an L-layered system that has D_z degrees of freedom in the zth layer. The layers are unrelated in general, but repeat periodically in lattice models. As usual, the full single-particle Green's function is $\tilde{G}_{\boldsymbol{k}}(\omega) = (\omega - \tilde{H}_{\boldsymbol{k}})^{-1}$ and has $\tilde{N} = \sum_{z=1}^{L} D_z$ poles corresponding to the eigenvalues $\tilde{\varepsilon}_{\boldsymbol{k},j}$, $j = 1 \ldots \tilde{N}$ of $\tilde{H}_{\boldsymbol{k}}$. The spectrum may have degeneracies and generically consists of three types of states: evanescent waves pinned to the top and the bottom surfaces and planes waves in the bulk.

Now, let us add a layer at $z = 0$ that we will refer to as the "surface." The full and effective surface Green's functions, respectively, are given by

$$G_{\boldsymbol{k}}(\omega) = \begin{pmatrix} \omega - H^S_{\boldsymbol{k}} & -h_{\boldsymbol{k}} \\ -h^\dagger_{\boldsymbol{k}} & \omega - \tilde{H}_{\boldsymbol{k}} \end{pmatrix}^{-1}, \tag{1}$$

$$g_{\boldsymbol{k}}(\omega) = \left(\omega - H^S_{\boldsymbol{k}} - h_{\boldsymbol{k}} \tilde{G}_{\boldsymbol{k}}(\omega) h^\dagger_{\boldsymbol{k}}\right)^{-1}, \tag{2}$$

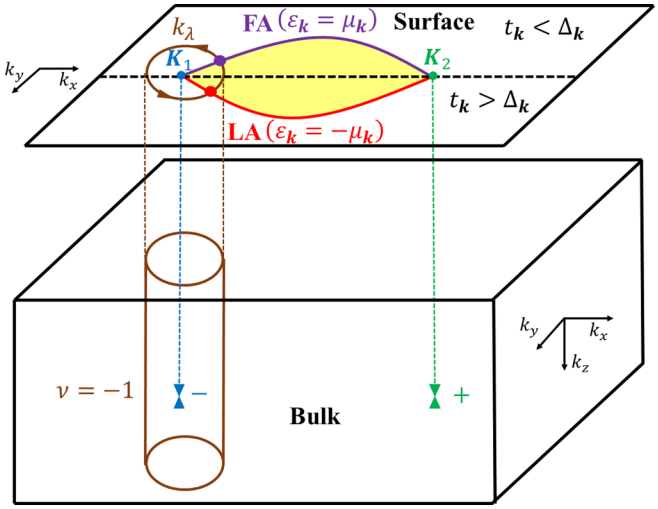

FIG. 1. Blue (green) cone and dot denotes the left- (right-)handed bulk Weyl node and its surface projection, respectively. While traversing a surface $\boldsymbol{k}$-space loop (brown curve parametrized by k_λ), the phase acquired by $g_{k_\lambda}(i0^+)$ on crossing the FA (purple curve) must be canceled by crossing a LA (red curve). The FA and LA form a closed loop and enclose a well-defined area (yellow region). The bulk extension of the k_λ curve defines a 2D insulator on the k_λ-k_z manifold (brown cylinder) with Chern number equal to the net chirality of the enclosed Weyl nodes. $\mathcal{E}_k$, μ_k, t_k, and Δ_k are parameters in the explicit model described later.

where H_k^S is the Bloch Hamiltonian of the surface layer and h_k, $h_k^\dagger$ capture coupling between the bulk and the surface and $g_k(\omega)$ is a matrix of dimension D_0. A standard identity for the determinant of a block matrix gives

$$\det g_k(\omega) = \frac{\det G_k(\omega)}{\det \tilde{G}_k(\omega)} = \frac{\prod_{i=1}^{\tilde{N}} (\omega - \tilde{\varepsilon}_{k,i})}{\prod_{j=1}^{N} (\omega - \varepsilon_{k,j})}. \tag{3}$$

Moreover, if interlayer hopping is sufficiently local, $\tilde{H}_k$ and H_k must have the same spectrum of evanescent waves on the $z = L$ surface up to exponentially small corrections in L. Thus, factors from such states cancel out in Eq. (3), leaving $\det g_k(\omega)$ to only depend on the bulk and top-surface spectra of H_k and $\tilde{H}_k$. Similarly to single-particle Green's functions in interacting systems [79], $\det g_k(\omega)$ is a ratio of zeros to poles, vanishes as $|\omega| \to \infty$, and is analytic away from the $\mathrm{Re}(\omega)$ axis.

Luttinger arcs. We now prove our main results, namely, the existence, connectivity, and detection of surface LAs by merely requiring $\det g_k(\omega)$ to be single valued. In particular, we prove that LAs (i) necessarily exist on the surface; (ii) connect Weyl node projections of opposite chirality, thus forming closed loops with the FAs; and (iii) can be precisely determined by peeling off suitable layers and measuring the new FAs. First, we derive the well-known existence of the FAs within a setup that facilitates the proof for LAs.

Consider a momentum space loop in the surface Brillouin zone, parametrized by k_λ, that does not pass through the surface projection of any Weyl node (Fig. 1). In the bulk, the surface defined by k_λ and k_z is a closed two-dimensional (2D) manifold. If the Weyl nodes are undoped, the manifold

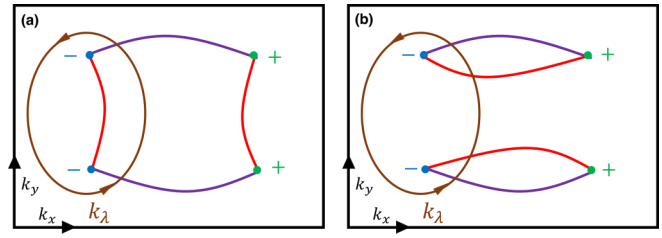

FIG. 2. Invalid (a) and valid (b) LA configurations, where LAs connect surface projections of Weyl nodes of the same and opposite chiralities, respectively.

has a gapped spectrum and can be viewed as a 2D Chern insulator with a Chern number ν equal to the net chirality of the enclosed Weyl nodes. The edge of this Chern insulator is the original k_λ loop on the WSM surface, so the loop must host a net of ν gapless, chiral modes, where each clockwise (counterclockwise) mode contributes $+1$ (-1) to ν. In other words, each right- (left-)handed Weyl node produces a FA state with a velocity component along the clockwise (counterclockwise) direction when viewed from above. In terms of Green's functions, each FA state corresponds to a vanishing nondegenerate eigenenergy $\varepsilon_{k_\lambda,j}$ for a certain j and contributes a simple pole to $g_k(\omega)$ at $\omega = 0$. Moreover, the *net* number of poles equals ν, where FAs with a velocity component antiparallel (parallel) to the loop direction contribute $+1$ (-1). The set of all possible loops on the WSM surface then traces out the FAs.

Now, consider the retarded surface Green's function, $g_k(\omega + i0^+)$. A necessary condition for it to be single valued is that the change in $\ln\det g_k(\omega + i0^+)$ vanishes around an arbitrary k_λ loop. Focusing on $\omega = 0$ and using Eq. (3),

$$\begin{aligned} 0 &= \oint d\boldsymbol{k}_\lambda \cdot \nabla \ln\det\left[g_k(i0^+)\right] \\ &= \pi\left(\sum_m \mathrm{sgn}\left[\tilde{v}_{k_m^{LA}}\right] - \sum_n \mathrm{sgn}\left[v_{k_n^{FA}}\right]\right), \end{aligned} \tag{4}$$

where k_m^{LA} (k_n^{FA}) are points on the k_λ loop where $\tilde{\varepsilon}_{k,i}$ $(\varepsilon_{k,j})$ vanishes for some i (j), while $\tilde{v}_k$ (v_k) is the projection of $\nabla\tilde{\varepsilon}_{k,j}(\nabla\varepsilon_{k,j})$ onto the loop direction. According to Eq. (3), $\det g_k(0)$ has zeros (poles) at these points. While the poles correspond to FAs and ensure $\sum_n \mathrm{sgn}[v_{k_n^{FA}}] = -\nu$ as argued above, Eq. (4) implies that $\sum_m \mathrm{sgn}[\tilde{v}_{k_m^{LA}}] = -\nu$ as well. In other words, there exist net ν zeros along the k_λ loop. The set of all $\boldsymbol{k}$-space loops yields strings of zeros, that are defined as the LAs. Intuitively, the phase acquired by $\det[g_k(i0^+)]$ upon crossing a FA must be canceled either by a FA of the opposite chirality or a LA of the same chirality to ensure $\det g_k(i0^+)$ is single valued. This implies that the LAs too connect surface projections of Weyl nodes of opposite chiralities and form closed loops with the FAs when the Weyl nodes are undoped. To illustrate this point, we show an invalid and a valid configuration in Fig. 2.

Detection by peeling. While Luttinger surfaces and arcs are common in strongly interacting systems, their shape is difficult to determine. There, a broad spectral function peak and low peak height reflect diverging self-energy and vanishing quasiparticle weight, respectively, but the precise point where the Green's function vanishes is inaccessible [84]. In contrast,

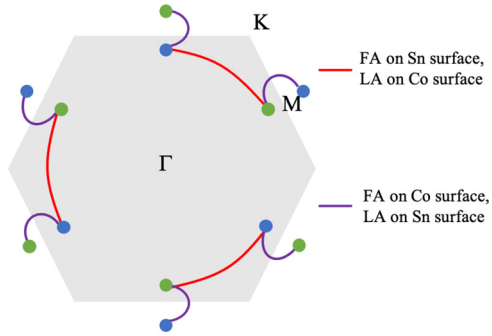

FIG. 3. Schematic of FAs and LAs on the surface of $Co_3Sn_2S_2$ for Co and Sn terminations. Gray region denotes the first Brillouin zone while blue and green dots are surface projections of Weyl nodes of opposite chirality.

we show that surface LAs in WSMs can be determined by simply peeling off the top layer and measuring the FAs on the new surface.

Suppose the L-layered system carries a FA that disappears upon adding another layer. This can only happen if the unit cell consists of more than one layer; otherwise the L- and $(L+1)$-layered systems would have the same FA spectrum as $L \to \infty$. The disappearance of FAs on adding a layer means there exists a string of $\boldsymbol{k}$ points such that $\tilde{\varepsilon}_{\boldsymbol{k},i} = 0$ for some i but $\varepsilon_{\boldsymbol{k},j} \neq 0\ \forall j$. According to Eq. (3), $\det g_{\boldsymbol{k}}(0) = 0$ along this curve, thus yielding a LA on the surface. Equivalently, the LA transforms into a FA when the surface layer is peeled off.

This principle readily reveals the locations of LAs on the surface of the ferromagnetic WSM $Co_3Sn_2S_2$ (Fig. 3). The crystal structure of $Co_3Sn_2S_2$ consists of Co kagome layers with a Sn at hexagon center separated by triangular layers of Sn and S [50,85–88]. Only three spinful Co d orbitals from the three kagome sites and a spinful p orbital from the Sn atoms between the kagome layers are near the Fermi level; bands from all other atoms and orbitals are far away in energy. As a result, the material is effectively a stack of bilayers consisting of Co-kagome and Sn-triangular layers. Recent tunneling measurements on the (001) surface discovered well-isolated FAs for Co and Sn terminations but with different connectivities [87]. We predict that the LAs on the Co (Sn) termination are simply the FAs on the Sn (Co) termination (Fig. 5). This result is immune to the detailed orbital content of wave functions and simply arises from the fact that LAs appear whenever FAs are annihilated by adding a layer.

In contrast, the peeling protocol cannot reveal LAs in the antiferromagnetic WSMs Mn_3Sn and Mn_3Ge [89–94]. These materials have a layered structure where each layer consists of a kagome lattice of Mn atoms with a Sn/Ge at the center of each kagome hexagon. Importantly, the layers are identical up to in-plane translations in real space, so termination at any layer results in the same surface Green's function in $\boldsymbol{k}$ space.

Effect of doping. So far, we have assumed every Weyl node to be at charge neutrality. Real WSMs typically contain Fermi pockets around Weyl nodes, which motivates an examination of the LAs under doping.

We first need to analyze the effect of the bulk states on $g_{\boldsymbol{k}}(\omega)$ more closely. When $L \to \infty$, the bulk spectrum at each 2D momentum $\boldsymbol{k}$ is continuous and indexed by k_z while both

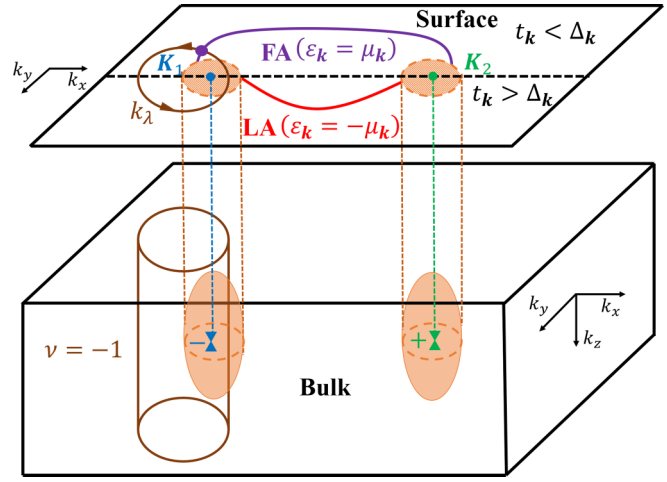

FIG. 4. Surface loops parametrized by k_λ exist that intersect the FA but avoid the LA. Along such a loop, the phase acquired by $\det g_{\boldsymbol{k}}(i0^+)$ on crossing the FA is canceled by traversing a patch where $\mathrm{Im}\det g_{\boldsymbol{k}}(i0^+)$ is finite. These patches (orange ellipses) are the surface projections of the bulk Fermi surfaces (orange ellipsoids).

$\tilde{G}_{\boldsymbol{k}}(\omega)$ and $G_{\boldsymbol{k}}(\omega)$ contain a continuum of poles on the $\mathrm{Re}(\omega)$ axis across the energy range spanned by the bulk bands at $\boldsymbol{k}$. Naively, one might expect the poles to cancel in Eq. (3) and leave $g_{\boldsymbol{k}}(\omega)$ without any additional features. However, for any finite L, the poles of $\tilde{G}_{\boldsymbol{k}}(\omega)$ and $G_{\boldsymbol{k}}(\omega)$ are generally distinct and typically separated by $O(1/L)$ due to k_z quantization. Crucially, $G_{\boldsymbol{k}}(\omega)$ has precisely $N - \tilde{N} = D_0$ more poles than $\tilde{G}_{\boldsymbol{k}}(\omega)$ does, D_0 being the number of degrees of freedom in the $z = 0$ layer. Thus, even in the limit $L \to \infty$, the contour integral $\oint d\omega \det g_{\boldsymbol{k}}(\omega)$ around the $\mathrm{Re}(\omega)$ axis is generically nonzero and finite, which suggests that $g_{\boldsymbol{k}}(\omega)$ develops branch cuts that span the bulk bands.

On the surface, doping creates patches of gapless states corresponding to surface projections of the bulk Fermi surfaces (Fig. 4). Consider a k_λ loop that intersects a FA and then crosses such a patch. When $\boldsymbol{k}$ is inside the patch, $\omega = 0$ lies within a branch cut of $g_{\boldsymbol{k}}(\omega)$, so $\mathrm{Im}\det g_{\boldsymbol{k}}(i0^+)$ is finite. Consequently, the sign change in $\det g_{\boldsymbol{k}}(0)$ upon crossing the FA gets gradually undone while traversing the patch without

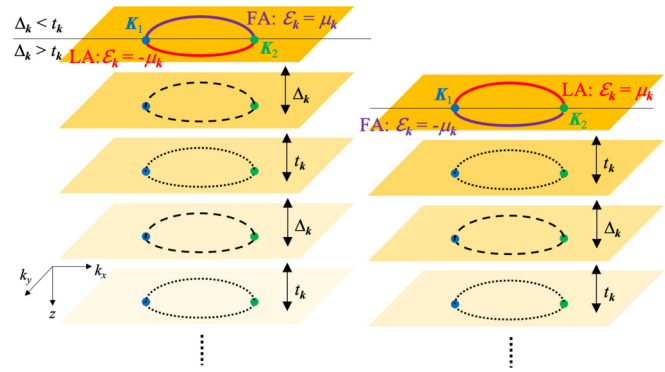

FIG. 5. In the bilayered WSM model, removing a layer interchanges the FA and the LA. Dashed (dotted) black curves denote electron (hole) Fermi surfaces that are the building blocks of the WSM (adapted from [42]; see text for details).

det $g_{\boldsymbol{k}}(0)$ vanishing anywhere along the loop. This causes the LA and the FA to separate while the patch fills the intervening region.

Explicit model. We now demonstrate our general results using an explicit model [42]. The model consists of a stack of spinless, alternating 2D electron and hole metals with Fermi surfaces given by phenomenological curves $\mathcal{E}_{\boldsymbol{k}} = \pm\mu_{\boldsymbol{k}}$. Interlayer couplings $-t_{\boldsymbol{k}} < 0$ and $\Delta_{\boldsymbol{k}} > 0$ cause each Fermi surface to hybridize preferentially with a layer above for certain $\boldsymbol{k}$ and a layer below for other $\boldsymbol{k}$. The Bloch Hamiltonian operator for the stack is $\hat{H}_{\boldsymbol{k}} = \sum_{z=0}^{L-1} \psi^\dagger_{z,\boldsymbol{k}}[-\mu_{\boldsymbol{k}} + (-1)^{z-1}\mathcal{E}_{\boldsymbol{k}}]\psi_{z,\boldsymbol{k}} + (\psi^\dagger_{z,\boldsymbol{k}} h_{zz+1,\boldsymbol{k}} \psi_{z+1,\boldsymbol{k}} + \text{H.c.})$, where $\psi^\dagger_{z,\boldsymbol{k}}$ creates an electron at 2D momentum $\boldsymbol{k}$ in the zth layer and $h_{zz+1,\boldsymbol{k}}$ equals $\Delta_{\boldsymbol{k}}$ $(-t_{\boldsymbol{k}})$ for even (odd) z. Fourier transforming $z \to k_z$ yields the bulk Bloch Hamiltonian and dispersion:

$$\mathcal{H}_{\boldsymbol{k}}(k_z) = \begin{pmatrix} -\mu_{\boldsymbol{k}} + \mathcal{E}_{\boldsymbol{k}} & \Delta_{\boldsymbol{k}} - t_{\boldsymbol{k}} e^{2ik_z c} \\ \Delta_{\boldsymbol{k}} - t_{\boldsymbol{k}} e^{-2ik_z c} & -\mu_{\boldsymbol{k}} - \mathcal{E}_{\boldsymbol{k}} \end{pmatrix},$$

$$\xi^{\pm}_{\boldsymbol{k}}(k_z) = -\mu_{\boldsymbol{k}} \pm \sqrt{\mathcal{E}^2_{\boldsymbol{k}} + \Delta^2_{\boldsymbol{k}} + t^2_{\boldsymbol{k}} - 2t_{\boldsymbol{k}}\Delta_{\boldsymbol{k}}\cos(2k_z c)}, \quad (5)$$

where c is the interlayer spacing. $\mathcal{H}_{\boldsymbol{k}}(k_z)$ has Weyl nodes at points $(\boldsymbol{K}_i, 0)$ where $t_{\boldsymbol{K}_i} = \Delta_{\boldsymbol{K}_i}$ and $\mathcal{E}_{\boldsymbol{K}_i} = \mu_{\boldsymbol{K}_i}$ and a gap elsewhere provided $|\mu_{\boldsymbol{k}}| < \epsilon_{\boldsymbol{k}-}$ $\forall \boldsymbol{k}$, where $\epsilon_{\boldsymbol{k}\pm} = \sqrt{\mathcal{E}^2_{\boldsymbol{k}} + (t_{\boldsymbol{k}} \pm \Delta_{\boldsymbol{k}})^2}$. If $\mu_{\boldsymbol{K}_i} = 0$, the ith Weyl node is at the Fermi level. Near $(\boldsymbol{K}_i, 0)$, $\mathcal{H}_{\boldsymbol{k}}(k_z) - \mu_{\boldsymbol{k}}$ reduces to $H_{\text{Weyl},i} = \boldsymbol{k}_{3D} \cdot (\boldsymbol{v}_i\sigma_z + \boldsymbol{u}_i\sigma_x + \boldsymbol{w}_i\sigma_y)$, where σ_α are Pauli matrices in the bilayer basis, $\boldsymbol{v}_i = \nabla_{\boldsymbol{k}}\mathcal{E}_{\boldsymbol{K}_i}$, $\boldsymbol{u}_i = \nabla_{\boldsymbol{k}}(\Delta_{\boldsymbol{K}_i} - t_{\boldsymbol{K}_i})$, and $\boldsymbol{w}_i = 2t_{\boldsymbol{K}_i} c\hat{\boldsymbol{z}} \equiv 2t_i c\hat{\boldsymbol{z}}$ are the Weyl velocities, and $\boldsymbol{k}_{3D} = (\boldsymbol{k}, k_z)$. On the top surface ($z = 0$), a FA exists along the $\mathcal{E}_{\boldsymbol{k}} = \mu_{\boldsymbol{k}}$ curve where $h_{12,\boldsymbol{k}} < h_{23,\boldsymbol{k}}$ or $\Delta_{\boldsymbol{k}} < t_{\boldsymbol{k}}$. Physically, the FA is the part of the 2D Fermi surface at $z = 0$ that survives because it has a propensity to hybridize with the missing layer at $z = -1$.

In this model, $D_0 = 1$, so the $g_{\boldsymbol{k}}(\omega)$ is a c number that has a closed-form expression in the limit $L \to \infty$ [42]:

$$g_{\boldsymbol{k}}(\omega) = \frac{1}{2t^2_{\boldsymbol{k}}(\omega + \mu_{\boldsymbol{k}} - \mathcal{E}_{\boldsymbol{k}})}\Big\{(\omega+\mu_{\boldsymbol{k}})^2 - \mathcal{E}^2_{\boldsymbol{k}} + t^2_{\boldsymbol{k}} - \Delta^2_{\boldsymbol{k}} + \sqrt{\big[(\omega+\mu_{\boldsymbol{k}})^2 - \epsilon^2_{\boldsymbol{k}-}\big]\big[(\omega+\mu_{\boldsymbol{k}})^2 - \epsilon^2_{\boldsymbol{k}+}\big]}\Big\}. \quad (6)$$

The FA and LA occur at $\mathcal{E}_{\boldsymbol{k}} = \mu_{\boldsymbol{k}}, t_{\boldsymbol{k}} > \Delta_{\boldsymbol{k}}$ and $\mathcal{E}_{\boldsymbol{k}} = -\mu_{\boldsymbol{k}}, t_{\boldsymbol{k}} < \Delta_{\boldsymbol{k}}$, respectively. Peeling off the $z = 0$ layer corresponds to the transformation $\mathcal{E}_{\boldsymbol{k}} \to -\mathcal{E}_{\boldsymbol{k}}$, $t_{\boldsymbol{k}} \leftrightarrow \Delta_{\boldsymbol{k}}$ in the semi-infinite limit, which interchanges the FAs and LAs as depicted in Fig. 5. Physically, the FA now exists along the part of the $z = 1$ Fermi surface that lacks a hybridization partner. Thanks to the square root, $g_{\boldsymbol{k}}(\omega)$ clearly has branch cuts when ω is real and lies within the bulk bands, i.e., $\epsilon_{\boldsymbol{k}-} < |\omega + \mu_{\boldsymbol{k}}| < \epsilon_{\boldsymbol{k}+}$. In Appendix A, we show that the branch cut reproduces the expected particle density on the surface due to the bulk states.

Implications for Luttinger's theorem. Luttinger's theorem is a hallmark of Fermi liquid theory. It states that the Luttinger volume —defined as the volume enclosed by the locus of poles of the electron Green's function—equals the density of spinful (spinless) electrons in a metal modulo 2 (modulo 1) in units of $(2\pi)^D$ in D spatial dimensions. Importantly, the theorem dictates that the Luttinger volume remains unchanged in the presence of interactions [76–82]. It was later generalized to include Mott insulators with particle-hole symmetry [79,81–84]. Here, a divergent self-energy produces a Luttinger surface that encloses a volume equal to the particle density modulo 2. In certain strongly interacting systems, Luttinger's theorem holds in a "soft" form as the Luttinger volume equals a fraction of the particle density modulo 2 [84,95–98]. Since there is no well-defined volume enclosed by the FAs alone in WSMs, Luttinger's theorem is naively inapplicable. However, the discovery of LAs in this work raises the question: Does the area enclosed by the Fermi-Luttinger loop act as a Luttinger volume and equal the surface particle density?

Using the minimal model described above, we prove that the answer is negative and quantify the violation of Luttinger's theorem. Restricting to $\mu_{\boldsymbol{k}} = 0$ for simplicity, the surface particle density at zero temperature is given by $n_s = -2\text{Im}\int_{\boldsymbol{k},\omega}\Theta(-\omega)g_{\boldsymbol{k}}(\omega + i\eta) = n^{\text{p}}_{\text{s}} + n^{\text{bc}}_{\text{s}}$ where

$$n^{\text{p}}_{\text{s}} = \int_{\boldsymbol{k}} \Theta(-\mathcal{E}_{\boldsymbol{k}}) R\left(1 - \frac{\Delta^2_{\boldsymbol{k}}}{t^2_{\boldsymbol{k}}}\right), \quad (7)$$

$$n^{\text{bc}}_{\text{s}} = \int_{\boldsymbol{k},\omega} \Theta(-\omega)\text{sgn}(\omega)\frac{\sqrt{R\big[(\omega^2 - \epsilon^2_{\boldsymbol{k}-})(\epsilon^2_{\boldsymbol{k}+} - \omega^2)\big]}}{t^2_{\boldsymbol{k}}(\omega - \mathcal{E}_{\boldsymbol{k}})} \quad (8)$$

denote contributions from the poles and the branch cuts of $g_{\boldsymbol{k}}(\omega)$, respectively, $\int_{\boldsymbol{k},\omega} \equiv \int \frac{d^2k\, d\omega}{(2\pi)^3}$ and $R(x) = x\Theta(x)$. In other words, n^{p}_{s} captures FA contributions to n_{s} and resembles the expression for the carrier density in a Fermi gas, but for the weight factor $W_{\boldsymbol{k}} = R(1 - \Delta^2_{\boldsymbol{k}}/t^2_{\boldsymbol{k}})$ that accounts for the varying weight of FA states on the surface and restricts contributions to the region containing FA's, namely, $\Delta_{\boldsymbol{k}} < t_{\boldsymbol{k}}$. In contrast, n^{bc}_{s} captures bulk contributions and approximates at $\mu = 0$ to (Appendix B)

$$n_{\text{s}} = \int_{\boldsymbol{k}} \Theta(-\mathcal{E}_{\boldsymbol{k}}) + O(t, \Delta)\nu_{\text{2D}}, \quad (9)$$

where ν_{2D} is the density of states at $\mathcal{E}_{\boldsymbol{k}} = 0$ for the 2D layers. The first term, $\int_{\boldsymbol{k}} \Theta(-\mathcal{E}_{\boldsymbol{k}})$, is precisely the area enclosed by the Fermi-Luttinger loop in units of $(2\pi)^2$ and can be viewed as a Luttinger volume (yellow region in Fig. 1). Physically, the equivalence at zeroth order in the interlayer tunnelings is a remnant of Luttinger's theorem that holds exactly for the 2D metals that form the building blocks of the WSM. The leading violation of the theorem is defined by the second term; it is order the typical interlayer tunneling and comes from $\boldsymbol{k}$-space regions near the Fermi-Luttinger loop, hence scaling as its circumference.

In conclusion, we have unearthed various novel features hidden in the surface single-particle Green's function of noninteracting WSMs. We have shown that the surface hosts LAs, normally found only in strongly interacting systems, in addition to FAs. When the Weyl nodes are undoped, the FAs and LAs form closed loops on the surface. Interestingly, the LA turns into a FA when the surface layer is removed, which allows a precise determination of the LAs. We use this principle to determine LAs in $Co_3Sn_2S_2$. Finally, we showed that doping the Weyl nodes exposes branch cuts in the

Green's function that capture the surface presence of the bulk bands.

Acknowledgments. We thank H. Pal for invaluable discussions. We acknowledge financial support from the National Science Foundation under Grant No. DMR-2047193.

APPENDIX A: n_s^{bc} INTEGRAL NEAR WEYL NODES, WITH DOPING

In this Appendix, we evaluate n_s^{bc} at nonzero but small $\mu_{\boldsymbol{k}}$ by linearizing around each Weyl node and compare it with the expected contribution of the bulk states to the surface particle density. We have

$$n_s^{bc} = \int_{\boldsymbol{k},\omega} \Theta(\mu_{\boldsymbol{k}} - \omega)\mathrm{sgn}(\omega) \frac{\sqrt{R\left[\left(\omega^2 - \epsilon_{\boldsymbol{k}-}^2\right)\left(\epsilon_{\boldsymbol{k}+}^2 - \omega^2\right)\right]}}{t_{\boldsymbol{k}}^2(\omega - \mathcal{E}_{\boldsymbol{k}})}, \tag{A1}$$

where $\epsilon_{\boldsymbol{k}\pm} = \sqrt{\mathcal{E}_{\boldsymbol{k}}^2 + (t_{\boldsymbol{k}} \pm \Delta_{\boldsymbol{k}})^2}$. The integrand is nonzero only when $\epsilon_{\boldsymbol{k}-} < |\omega| < \epsilon_{\boldsymbol{k}+}$, which defines a region around each Weyl node within an energy $|\omega|$ from the node. As long as the contributing regions around different nodes do not overlap in $\boldsymbol{k}$ space, the $\boldsymbol{k}$ integral can be split into integrals around each node:

$$n_s^{bc} = \int_\omega \sum_i \int_{\boldsymbol{k}\approx\boldsymbol{K}_i} \Theta(\mu_{\boldsymbol{k}} - \omega)\mathrm{sgn}(\omega) \times \frac{\sqrt{R\left[\left(\omega^2 - \epsilon_{\boldsymbol{k}-}^2\right)\left(\epsilon_{\boldsymbol{k}+}^2 - \omega^2\right)\right]}}{t_{\boldsymbol{k}}^2(\omega - \mathcal{E}_{\boldsymbol{k}})}, \tag{A2}$$

where $\boldsymbol{K}_i$ are the locations of the Weyl nodes. Near each node, let us linearize as $\mathcal{E}_{\boldsymbol{k}} \approx \boldsymbol{k}\cdot\boldsymbol{v}_i$, $t_{\boldsymbol{k}} \approx t_i - \frac{1}{2}\boldsymbol{k}\cdot\boldsymbol{u}_i$, $\Delta_{\boldsymbol{k}} \approx t_i + \frac{1}{2}\boldsymbol{k}\cdot\boldsymbol{u}_i$ and assume $2t_i \gg\equiv |\mu_i|$, where μ_i is the Fermi level relative to the ith Weyl node. For simplicity, we ignore tilting of the linear dispersion by neglecting linear terms in the Taylor expansion of $\mu_{\boldsymbol{k}}$ around $\boldsymbol{K}_i$. Subtracting off an infinite contribution from $\mu_i = 0$, we get

$$\Delta n_s^{bc} = \sum_i \int_0^{|\mu_i|} \frac{d\omega}{2\pi} \int_{\sqrt{(\boldsymbol{k}\cdot\boldsymbol{v}_i)^2 + (\boldsymbol{k}\cdot\boldsymbol{u}_i)^2} < \omega} \frac{d^2k}{(2\pi)^2} \times \frac{2\sqrt{\omega^2 - (\boldsymbol{k}\cdot\boldsymbol{v}_i)^2 - (\boldsymbol{k}\cdot\boldsymbol{u}_i)^2}}{t_i[\omega\,\mathrm{sgn}(\mu_i) - \boldsymbol{k}\cdot\boldsymbol{v}_i]}. \tag{A3}$$

The integral simplifies upon absorbing the velocities into the momenta as $q_v = \boldsymbol{k}\cdot\boldsymbol{v}_i = q\,\cos\phi$, $q_u = \boldsymbol{k}\cdot\boldsymbol{u}_i = q\,\sin\phi$:

$$\Delta n_s^{bc} = \sum_i \int_0^{|\mu_i|} \frac{d\omega}{2\pi} \frac{2}{t_i u_i v_i} \times \int_{q<|\omega|} \frac{q\,dq\,d\phi}{(2\pi)^2} \frac{\sqrt{\omega^2 - q^2}}{\omega\,\mathrm{sgn}(\mu_i) - q\,\cos\phi} \tag{A4}$$

$$= \sum_i \frac{2\,\mathrm{sgn}(\mu_i)}{t_i u_i v_i} \int_0^{|\mu_i|} \frac{d\omega}{2\pi} \int_0^{\omega} \frac{q\,dq}{2\pi} \tag{A5}$$

$$= \frac{2}{3}\pi \sum_i \left(\frac{\mu_i}{2\pi}\right)^3 \frac{1}{t_i u_i v_i}. \tag{A6}$$

In comparison, the change in the 3D bulk carrier density around a Weyl node with velocities u_i, v_i, and w_i due to a local chemical potential μ_i follows easily from the volume of an ellipsoid:

$$\Delta N_i^{\mathrm{Weyl}} = \frac{4}{3}\pi\left(\frac{\mu_i}{2\pi}\right)^3 \frac{1}{u_i v_i w_i}. \tag{A7}$$

Recalling that $w_i = 2t_i c$, we find $\Delta n_s^{bc} = c\sum_i \Delta N_i^{\mathrm{Weyl}}$, i.e., Δn_s^{bc} reflects the change in the bulk carrier density uniformly distributed across the layers. Thus, the branch cut in $g_{\boldsymbol{k}}(\omega)$ is a manifestation of the continuum of bulk quasiparticle poles at fixed $\boldsymbol{k}$ and varying k_z.

APPENDIX B: n_s^{bc} INTEGRALS AT GENERAL k, NO DOPING

In this appendix, we separately evaluate contributions from $\boldsymbol{k}$ points where $\mathcal{E}_{\boldsymbol{k}} < 0$ ($n_{s,-}^{bc}$), $\mathcal{E}_{\boldsymbol{k}} \approx 0$ ($n_{s,0}^{bc}$), and $\mathcal{E}_{\boldsymbol{k}} > 0$ ($n_{s,+}^{bc}$) to obtain $n_s^{bc} = n_{s,-}^{bc} + n_{s,0}^{bc} + n_{s,+}^{bc}$ at $\mu_{\boldsymbol{k}} = 0$, as needed for quantifying the violation of Luttinger's theorem based on the area enclosed by the Fermi-Luttinger loop.

1. $n_{s,-}^{bc}$

If $|t_{\boldsymbol{k}}, \Delta_{\boldsymbol{k}}| < -\mathcal{E}_{\boldsymbol{k}}$, then $\omega \approx \mathcal{E}_{\boldsymbol{k}}$ over the range of the ω integral and $1/(\omega - \mathcal{E}_{\boldsymbol{k}}) = 2\omega/(\omega^2 - \mathcal{E}_{\boldsymbol{k}}^2) + O(\frac{t^2,\Delta^2,t\Delta}{\mathcal{E}^2})$. The leading order term is a straightforward elliptic integral in terms of $x = \omega^2 - \mathcal{E}_{\boldsymbol{k}}^2$:

$$\begin{aligned} n_{s,-}^{bc}(0) &= \int_{\boldsymbol{k}} \frac{\Theta(-\mathcal{E}_{\boldsymbol{k}})}{2\pi t_{\boldsymbol{k}}^2} \times \int_{t_{\boldsymbol{k}-}^2}^{t_{\boldsymbol{k}+}^2} dx \frac{\sqrt{(x - |t_{\boldsymbol{k}} - \Delta_{\boldsymbol{k}}|^2)(|t_{\boldsymbol{k}} + \Delta_{\boldsymbol{k}}|^2 - x)}}{x} \\ &= \int_{\boldsymbol{k}} \frac{\Theta(-\mathcal{E}_{\boldsymbol{k}})}{4t_{\boldsymbol{k}}^2}(|t_{\boldsymbol{k}} + \Delta_{\boldsymbol{k}}| - |t_{\boldsymbol{k}} - \Delta_{\boldsymbol{k}}|)^2 \\ &= \int_{\boldsymbol{k}} (1 - W_{\boldsymbol{k}}). \end{aligned} \tag{B1}$$

2. $n_{s,0}^{bc}$

If $|t_{\boldsymbol{k}}, \Delta_{\boldsymbol{k}}| \gg |\mathcal{E}_{\boldsymbol{k}}|$, corresponding to the region near the Fermi and Luttinger arcs, we can restrict to a narrow region of width $O(t, \Delta)$ around the $\mathcal{E}_{\boldsymbol{k}} = 0$ contour. This gives

$$\begin{aligned} n_{s,0}^{bc}(0) &\approx \int_{\boldsymbol{k}} \frac{O(t,\Delta)\delta(\mathcal{E}_{\boldsymbol{k}})}{2\pi t_{\boldsymbol{k}}^2} \times \int_{-\epsilon_{\boldsymbol{k}+}}^{-\epsilon_{\boldsymbol{k}-}} d\omega \frac{\sqrt{(\omega^2 - |t_{\boldsymbol{k}} - \Delta_{\boldsymbol{k}}|^2)(|t_{\boldsymbol{k}} + \Delta_{\boldsymbol{k}}|^2 - \omega^2)}}{\omega} \\ &= \int_{\boldsymbol{k}} \frac{O(t,\Delta)\delta(\mathcal{E}_{\boldsymbol{k}})}{8t_{\boldsymbol{k}}^2}(|t_{\boldsymbol{k}} + \Delta_{\boldsymbol{k}}| - |t_{\boldsymbol{k}} - \Delta_{\boldsymbol{k}}|)^2 \\ &= \frac{1}{2}\int_{\boldsymbol{k}} O(t,\Delta)\delta(\mathcal{E}_{\boldsymbol{k}})(1 - W_{\boldsymbol{k}}). \end{aligned} \tag{B2}$$

Due to the δ function, this term receives contributions from regions near the Fermi-Luttinger loop only. It is $O(t, \Delta)\nu_{2D}$

and constitutes the leading violation of Luttinger's theorem based on the Fermi-Luttinger loop.

3. $n^{\rm bc}_{s,+}$

If $0 < |t_k, \Delta_k| \ll \mathcal{E}_k$, we can approximate $1/(\omega - \mathcal{E}_k) \approx 1/2\omega$. This gives an elliptic integral in terms of $x = \omega^2$ which evaluates to

$$n^{\rm bc}_{s,+}(0) \approx \int_{k,\mathcal{E}\gg|t,\Delta|} \int_{\epsilon^2_{k-}}^{\epsilon^2_{k+}} dx \frac{\sqrt{(x-\epsilon^2_{k-})(\epsilon^2_{k+}-x)}}{8\pi t^2_k x} \approx -\int_{k,\mathcal{E}\gg|t,\Delta|} \frac{\Delta^2_k}{4\mathcal{E}^2_k}. \tag{B3}$$

[1] O. Vafek and A. Vishwanath, Annu. Rev. Condens. Matter Phys. **5**, 83 (2014).
[2] A. A. Burkov, Annu. Rev. Condens. Matter Phys. **9**, 359 (2018).
[3] A. A. Burkov, Nat. Mater. **15**, 1145 (2016).
[4] B. Yan and C. Felser, Annu. Rev. Condens. Matter Phys. **8**, 337 (2017).
[5] N. P. Armitage, E. J. Mele, and A. Vishwanath, Rev. Mod. Phys. **90**, 015001 (2018).
[6] S.-Q. Shen, *Topological Insulators* (Springer, Singapore, 2017)
[7] I. Belopolski, D. S. Sanchez, Y. Ishida, X. Pan, P. Yu, S.-Y. Xu, G. Chang, T.-R. Chang, H. Zheng, N. Alidoust *et al.*, Nat. Commun. **7**, 13643 (2016).
[8] Z. P. Guo, P. C. Lu, T. Chen, J. F. Wu, J. Sun, and D. Y. Xing, Sci. China: Phys., Mech. Astron. **61**, 038211 (2018).
[9] G. Chang, S.-Y. Xu, H. Zheng, C.-C. Lee, S.-M. Huang, I. Belopolski, D. S. Sanchez, G. Bian, N. Alidoust, T.-R. Chang *et al.*, Phys. Rev. Lett. **116**, 066601 (2016).
[10] A. Gyenis, H. Inoue, S. Jeon, B. B. Zhou, B. E. Feldman, Z. Wang, J. Li, S. Jiang, Q. D. Gibson, S. K. Kushwaha *et al.*, New J. Phys. **18**, 105003 (2016).
[11] S.-M. Huang, S.-Y. Xu, I. Belopolski, C.-C. Lee, G. Chang, B. Wang, N. Alidoust, G. Bian, M. Neupane, C. Zhang *et al.*, Nat. Commun. **6**, 7373 (2015).
[12] H. Inoue, A. Gyenis, Z. Wang, J. Li, S. W. Oh, S. Jiang, N. Ni, B. A. Bernevig, and A. Yazdani, Science **351**, 1184 (2016).
[13] B. Q. Lv, N. Xu, H. M. Weng, J. Z. Ma, P. Richard, X. C. Huang, L. X. Zhao, G. F. Chen, C. E. Matt, F. Bisti *et al.*, Nat. Phys. **11**, 724 (2015).
[14] Y. Sun, S. C. Wu, and B. Yan, Phys. Rev. B **92**, 115428 (2015).
[15] S.-Y. Xu, I. Belopolski, N. Alidoust, M. Neupane, G. Bian, C. Zhang, R. Sankar, G. Chang, Z. Yuan, C.-C. Lee *et al.*, Science **349**, 613 (2015).
[16] S. Y. Xu, I. Belopolski, D. S. Sanchez, M. Neupane, G. Chang, K. Yaji, Z. Yuan, C. Zhang, K. Kuroda, G. Bian *et al.*, Phys. Rev. Lett. **116**, 096801 (2016).
[17] L. X. Yang, Z. K. Liu, Y. Sun, H. Peng, H. F. Yang, T. Zhang, B. Zhou, Y. Zhang, Y. F. Guo, M. Rahn *et al.*, Nat. Phys. **11**, 728 (2015).
[18] H. Zheng, S. Y. Xu, G. Bian, C. Guo, G. Chang, D. S. Sanchez, I. Belopolski, C. C. Lee, S. M. Huang, X. Zhang *et al.*, ACS Nano **10**, 1378 (2016).
[19] P. Hosur and X. Qi, C. R. Phys. **14**, 857 (2013).
[20] H. Wang and J. Wang, Chin. Phys. B **27**, 107402 (2018).
[21] J. Hu, S.-Y. Xu, N. Ni, and Z. Mao, Annu. Rev. Mater. Res. **49**, 207 (2019).
[22] A. A. Zyuzin and A. A. Burkov, Phys. Rev. B **86**, 115133 (2012).
[23] Y. Chen, S. Wu, and A. A. Burkov, Phys. Rev. B **88**, 125105 (2013).
[24] M. M. Vazifeh and M. Franz, Phys. Rev. Lett. **111**, 027201 (2013).
[25] A. A. Burkov, J. Phys.: Condens. Matter **27**, 113201 (2015).
[26] P. Hosur, S. Parameswaran, and A. Vishwanath, Phys. Rev. Lett. **108**, 046602 (2012).
[27] F. de Juan, A. G. Grushin, T. Morimoto, and J. E. Moore, Nat. Commun. **8**, 15995 (2017).
[28] S. Wang, B. C. Lin, A. Q. Wang, D. P. Yu, and Z. M. Liao, Adv. Phys.: X **2**, 518 (2017).
[29] N. Nagaosa, T. Morimoto, and Y. Tokura, Nat. Rev. Mater. **5**, 621 (2020).
[30] H. B. Nielsen and M. Ninomiya, Phys. Lett. B **130**, 389 (1983).
[31] M. V. Isachenkov and A. V. Sadofyev, Phys. Lett. B **697**, 404 (2011).
[32] A. V. Sadofyev, V. I. Shevchenko, and V. I. Zakharov, Phys. Rev. D **83**, 105025 (2011).
[33] R. Loganayagam and P. Surówka, J. High Energy Phys. **2012**, 97 (2012).
[34] P. Goswami and S. Tewari, Phys. Rev. B **88**, 245107 (2013).
[35] Z. Wang and S.-C. Zhang, Phys. Rev. B **87**, 161107(R) (2013).
[36] G. Basar, D. E. Kharzeev, and H.-U. Yee, Phys. Rev. B **89**, 035142 (2014).
[37] K. Landsteiner, Phys. Rev. B **89**, 075124 (2014).
[38] E. Benito-Matías and R. A. Molina, Phys. Rev. B **99**, 075304 (2019).
[39] P. Deng, Z. Xu, K. Deng, K. Zhang, Y. Wu, H. Zhang, S. Zhou, and X. Chen, Phys. Rev. B **95**, 245110 (2017).
[40] K. Deng, G. Wan, P. Deng, K. Zhang, S. Ding, E. Wang, M. Yan, H. Huang, H. Zhang, Z. Xu *et al.*, Nat. Phys. **12**, 1105 (2016).
[41] F. Haldane, arXiv:1401.0529.
[42] P. Hosur, Phys. Rev. B **86**, 195102 (2012).
[43] L. Huang, T. M. McCormick, M. Ochi, Z. Zhao, M. T. Suzuki, R. Arita, Y. Wu, D. Mou, H. Cao, J. Yan *et al.*, Nat. Mater. **15**, 1155 (2016).
[44] D. Iaia, G. Chang, T.-R. Chang, J. Hu, Z. Mao, H. Lin, S. Yan, and V. Madhavan, npj Quantum Mater. **3**, 38 (2018).
[45] H. Kwon, T. Jeong, S. Appalakondaiah, Y. Oh, I. Jeon, H. Min, S. Park, Y. J. Song, E. Hwang, and S. Hwang, Nano Res. **13**, 2534 (2020).
[46] A. Lau, K. Koepernik, J. van den Brink, and C. Ortix, Phys. Rev. Lett. **119**, 076801 (2017).
[47] M. Sakano, M. S. Bahramy, H. Tsuji, I. Araya, K. Ikeura, H. Sakai, S. Ishiwata, K. Yaji, K. Kuroda, A. Harasawa *et al.*, Phys. Rev. B **95**, 121101(R) (2017).
[48] S. Y. Xu, I. Belopolski, D. S. Sanchez, C. Zhang, G. Chang, C.

Guo, G. Bian, Z. Yuan, H. Lu, T. R. Chang *et al.*, Sci. Adv. **1**, 1501092 (2015).
[49] S. Y. Xu, C. Liu, S. K. Kushwaha, R. Sankar, J. W. Krizan, I. Belopolski, M. Neupane, G. Bian, N. Alidoust, T. R. Chang *et al.*, Science **347**, 294 (2015).
[50] Q. Xu, E. Liu, W. Shi, L. Muechler, J. Gayles, C. Felser, and Y. Sun, Phys. Rev. B **97**, 235416 (2018).
[51] Y. Yuan, X. Yang, L. Peng, Z.-J. Wang, J. Li, C.-J. Yi, J.-J. Xian, Y.-G. Shi, and Y.-S. Fu, Phys. Rev. B **97**, 165435 (2018).
[52] C. Zhang, A. Narayan, S. Lu, J. Zhang, H. Zhang, Z. Ni, X. Yuan, Y. Liu, J.-H. Park, E. Zhang *et al.*, Nat. Commun. **8**, 1272 (2017).
[53] Q.-Q. Yuan, L. Zhou, Z.-C. Rao, S. Tian, W.-M. Zhao, C.-L. Xue, Y. Liu, T. Zhang, C.-Y. Tang, Z.-Q. Shi *et al.*, Sci. Adv. **5**, aaw9485 (2019).
[54] P. J. W. Moll, N. L. Nair, T. Helm, A. C. Potter, I. Kimchi, A. Vishwanath, and J. G. Analytis, Nature (London) **535**, 266 (2016).
[55] A. C. Potter, I. Kimchi, and A. Vishwanath, Nat. Commun. **5**, 5161 (2014).
[56] Y. Zhang, D. Bulmash, P. Hosur, A. Potter, and A. Vishwanath, Sci. Rep. **6**, 23741 (2016).
[57] M. Z. Hasan and C. L. Kane, Rev. Mod. Phys. **82**, 3045 (2010).
[58] X.-L. Qi and S.-C. Zhang, Rev. Mod. Phys. **83**, 1057 (2011).
[59] R. S. K. Mong and V. Shivamoggi, Phys. Rev. B **83**, 125109 (2011).
[60] J. Borchmann and T. Pereg-Barnea, Phys. Rev. B **96**, 125153 (2017).
[61] Y. Zhang, Phys. Rev. Research **1**, 022005(R) (2019).
[62] S. Nishihaya, M. Uchida, Y. Nakazawa, M. Kriener, Y. Taguchi, and M. Kawasaki, Nat. Commun. **12**, 2572 (2021).
[63] C. Zhang, Y. Zhang, X. Yuan, S. Lu, J. Zhang, A. Narayan, Y. Liu, H. Zhang, Z. Ni, R. Liu *et al.*, Nature (London) **565**, 331 (2019).
[64] Ž. B. Lošić, J. Phys.: Condens. Matter **30**, 365003 (2018).
[65] O. V. Bugaiko, E. V. Gorbar, and P. O. Sukhachov, Phys. Rev. B **102**, 085426 (2020).
[66] E. V. Gorbar, V. A. Miransky, I. A. Shovkovy, and P. O. Sukhachov, Phys. Rev. B **99**, 155120 (2019).
[67] J. Hofmann and S. Das Sarma, Phys. Rev. B **93**, 241402(R) (2016).
[68] T. Tamaya, T. Kato, K. Tsuchikawa, S. Konabe, and S. Kawabata, J. Phys.: Condens. Matter **31**, 305001 (2019).
[69] J. C. W. Song and M. S. Rudner, Phys. Rev. B **96**, 205443 (2017).
[70] G. M. Andolina, F. M. D. Pellegrino, F. H. L. Koppens, and M. Polini, Phys. Rev. B **97**, 125431 (2018).
[71] F. Adinehvand, Z. Faraei, T. Farajollahpour, and S. A. Jafari, Phys. Rev. B **100**, 195408 (2019).
[72] S. Ghosh and C. Timm, Phys. Rev. B **101**, 165402 (2020).
[73] Z. Faraei and S. A. Jafari, Phys. Rev. B **100**, 035447 (2019).
[74] C. Huang, B. T. Zhou, H. Zhang, B. Yang, R. Liu, H. Wang, Y. Wan, K. Huang, Z. Liao, E. Zhang *et al.*, Nat. Commun. **10**, 1 (2019).
[75] U. Khanna, A. Kundu, S. Pradhan, and S. Rao, Phys. Rev. B **90**, 195430 (2014).
[76] K. B. Blagoev and K. S. Bedell, Phys. Rev. Lett. **79**, 1106 (1997).
[77] J. M. Luttinger, Phys. Rev. **119**, 1153 (1960).
[78] M. Oshikawa, Phys. Rev. Lett. **84**, 3370 (2000).
[79] K. Seki and S. Yunoki, Phys. Rev. B **96**, 085124 (2017).
[80] J. Voit, Rep. Prog. Phys. **58**, 977 (1995).
[81] M. Yamanaka, M. Oshikawa, and I. Affleck, Phys. Rev. Lett. **79**, 1110 (1997).
[82] J. T. Heath and K. S. Bedell, New J. Phys. **22**, 063011 (2020).
[83] I. Dzyaloshinskii, Phys. Rev. B **68**, 085113 (2003).
[84] T. D. Stanescu, P. Phillips, and T.-P. Choy, Phys. Rev. B **75**, 104503 (2007).
[85] Y. Okamura, S. Minami, Y. Kato, Y. Fujishiro, Y. Kaneko, J. Ikeda, J. Muramoto, R. Kaneko, K. Ueda, V. Kocsis *et al.*, Nat. Commun. **11**, 4619 (2020).
[86] D. F. Liu, A. J. Liang, E. K. Liu, Q. N. Xu, Y. W. Li, C. Chen, D. Pei, W. J. Shi, S. K. Mo, P. Dudin *et al.*, Science **365**, 1282 (2019).
[87] N. Morali, R. Batabyal, P. K. Nag, E. Liu, Q. Xu, Y. Sun, B. Yan, C. Felser, N. Avraham, and H. Beidenkopf, Science **365**, 1286 (2019).
[88] S. N. Guin, P. Vir, Y. Zhang, N. Kumar, S. J. Watzman, C. Fu, E. Liu, K. Manna, W. Schnelle, J. Gooth *et al.*, Adv. Mater. **31**, 1806622 (2019).
[89] H. Yang, Y. Sun, Y. Zhang, W.-J. Shi, S. S. P. Parkin, and B. Yan, New J. Phys. **19**, 015008 (2017).
[90] T. Matsuda, N. Kanda, T. Higo, N. P. Armitage, S. Nakatsuji, and R. Matsunaga, Nat. Commun. **11**, 909 (2020).
[91] T. Higo, D. Qu, Y. Li, C. L. Chien, Y. Otani, and S. Nakatsuji, Appl. Phys. Lett. **113**, 202402 (2018).
[92] T. Chen, T. Tomita, S. Minami, M. Fu, T. Koretsune, M. Kitatani, I. Muhammad, D. Nishio-Hamane, R. Ishii, F. Ishii *et al.*, Nat. Commun. **12**, 572 (2021).
[93] X. Wang, D. Pan, Q. Zeng, X. Chen, H. Wang, D. Zhao, Z. Xu, Q. Yang, J. Deng, T. Zhai *et al.*, Nanoscale **13**, 2601 (2021).
[94] J. Kübler and C. Felser, Europhys. Lett. **120**, 47002 (2017).
[95] P. W. Phillips, B. W. Langley, and J. A. Hutasoit, Phys. Rev. B **88**, 115129 (2013).
[96] B. Padhi, C. Setty, and P. W. Phillips, Nano Lett. **18**, 6175 (2018).
[97] K. Limtragool, Z. Leong, and P. W. Phillips, SciPost Phys. **5**, 049 (2018).
[98] K. B. Dave, P. W. Phillips, and C. L. Kane, Phys. Rev. Lett. **110**, 090403 (2013).